International Global Navigation Satellite Systems Association
IGNSS Conference 2016

Colombo Theatres, Kensington Campus, UNSW Australia
6 – 8 December 2016

Real-time Cycle Slip Detection and Repair for Network Multi-GNSS, Multi-frequency data processing

Tao Li (1)
Cooperative Research Centre for Spatial Information, Melbourne, Australia
Geoscience Australia, Canberra, Australia
+61 (2) 6249 9510 Tao.Li@ga.gov.au

Stavros Melachroinos (2)
Geoscience Australia, Canberra, Australia
+61 (2) 6249 9479 Stavros.Melachroinos@ga.gov.au

ABSTRACT

The GNSS community is experiencing a new era with the development of the multi-GNSS and multi-frequency industry. For high-precision GNSS data processing with the use of carrier phase measurements, quality control steps, such as, cycle slip detection and repair, are essential. With the correct detection and repair of the cycle slips, the carrier phase measurements will not be lumped by the unknown integer jumps. Therefore repeated integer ambiguity resolution in RTK or long convergence time in PPP, or PPP-RTK, will be avoided, especially in the extreme case of full loss of all the signals. In this contribution, a cycle slip detection and repair procedure, which has been implemented into our real-time Analysis Centre Software (ACS) pre-processing and data editing (PDE) function, is presented. At first, the noise levels of Hatch-Melbourne-Wübbena (MW) and Extra MW (EMW) linear combinations are investigated. The cycle slip detection approaches based on linear combinations and quality control theory under statistical hypothesis testing are then comparatively studied with multi-GNSS and multi-frequency data. As soon as the cycle slips are detected, mathematical and stochastic models for cycle slip repair are established. These models rely on time-differenced code and carrier phase measurements, as well as prior knowledge of the time-differenced ionosphere residual. The least-squares estimation is used to estimate the unknown parameters and their variance-covariance matrix. The float cycle slips and their variance covariance matrix are then used to reliably repair the cycle slips based on Integer Least-squares (ILS) estimation. Overall, the numerical results indicate the effectiveness of the implemented method for real-time network multi-GNSS and multi-frequency data processing. Moreover, the benefits of the triple-frequency cycle slip detection and repair algorithm are demonstrated.

KEYWORDS: GNSS; Cycle Slip; Detection, Repair; Triple-Frequency

1. INTRODUCTION

Precise positioning algorithms that perform integer ambiguity resolution rely on continuous carrier phase tracking without cycle slips (CS) in order to achieve centimetre- to millimetre-level positioning results. As soon as the integer ambiguities are resolved, the carrier phase measurements begin to continuously act as range measurements with millimetre level accuracy. However, when a CS occurs, which is caused by the loss of signal due to line-of-sight blockage, dynamic stress or signal interference, the resolved integer ambiguities will be lumped with the unknown integer CSs and the carrier phase measurements will be biased by at least one cycle (~20cm). Therefore, the integer CSs are required to be detected and repaired in order to recover the continuity of the carrier phase measurements.

There have been numerous publications on CS detection and repair algorithms, such as linear combination (LC) oriented algorithms in Blewitt (1990), Gao and Li (1999), Bisnath and Langley (2000), Kim and Langley (2001), de Lacy et al (2008), Liu (2011) and Zhao et al. (2015). These methods are based on forming LCs with certain properties to perform the detection, such as the widely used Hatch-Melbourne-Wübbena (MW) (Hatch 1983; Melbourne 1985; Wübbena 1985) for dual-frequency measurements or Extra Hatch-Melbourne-Wübbena (EMW) (Zhao et al 2015) for triple-frequency measurements and the Geometry-free (GF). Once the CSs are detected using the LCs, the repair step is usually performed by using the integer rounding method, which basically rounds the float CSs to their nearest integers.

Another methodology is to treat the CSs as outliers and detect them based on the quality control (QC) theory (Baarda 1968, Teunissen 1990), as researched in Teunissen and de Bakker (2013, 2015) and Banville and Langley (2013). The detection step is accomplished by a Local Overall Model (LOM) testing based on the statistics of the residuals (Odijk and Verhagen 2007). After successful CS detection, the alternative hypothesis is adopted to build the mathematical models and the Integer Least-squares (ILS) estimation is used to repair the CSs. The ILS is optimal in terms of maximizing the success-rate of integer ambiguity resolution (Teunissen 1998). This principal has been investigated in Teunissen and de Bakker (2015), Banville and Langley (2013) and Zhang and Li (2015). Most of these studies were not applied in the real-time network domain.

Under the context of our real-time multi-GNSS, multi-frequency Analysis Centre Software (ACS) pre-processing data editing (PDE) function, the CS detection and repair algorithms have been implemented and their performance have been studied. The reliability of the CS detection and repair steps using EMW and MW linear combinations are analysed first. Then the actual performance of the algorithms is evaluated by introducing artificial CSs on the raw data. The LC-based algorithm and the QC-based algorithm are comparatively studied, for dual-frequency and triple-frequency scenarios. Subsequently, the ILS success-rates of the repair-step are analysed against the satellite elevation, and at the final section, conclusions and recommendations are presented.

2. The CS DETECTION AND REPAIR ALGORITHMS

In the following, the detection and repair algorithms will be discussed and studied with dual- and triple-frequency multi-GNSS measurements.

2.1 The CS Detection step

Essentially, the CSs are detected before conducting the repair step. The CS detection method is based on the time-differenced (TD) code and phase measurements, which can be described as:

$$\Delta L_i = \Delta\rho - u_i \Delta I + \lambda_i \Delta N_i + \Delta\varepsilon_i \quad (1)$$
$$\Delta P_i = \Delta\rho + u_i \Delta I + \Delta v_i \quad (2)$$

where L and P are the phase and code measurements in unit of meter. Δ is the time-differencing operator between two consecutive epochs, ρ represents the non-dispersive delay. $u_i = (f_1^2)/(f_i^2)$ is the ionosphere coefficients on the ith frequency f_i, I is the first-order ionospheric delay, λ and N are the wavelength and ambiguities and ΔN is the TD ambiguities (integer CSs), ε and v are the measurement residuals, with the noises as σ_L and σ_P, respectively. The noise for each frequency is assumed to be the same. In terms of multi-GNSS and multi-frequency, the triple-frequency indices L_1, L_2 and L_5 are used which correspond to : GPS, and QZSS L1, L2 and L5 bands, GLONASS L1, L2 and L3 bands, BDS B1, B2 and B3 bands and Galileo E1, E5a and E5b bands. If no CS occurs, ΔN is 0 for each frequency.

The instrumental delays between two consecutive epochs are assumed to be absent since they remain quite stable over a short period of time (Liu et al. 2004). Based on equations (1) and (2), the CS detection algorithms are classified into LC-based approach and QC-based approach. In the following, these two approaches are going to be introduced.

LC approach

In case only dual-frequency measurements are available, the TD MW LC can be used to detect the CSs as:

$$\Delta N_{mw} = \left(\frac{f_1 \Delta L_1 - f_2 \Delta L_2}{f_1 - f_2} - \frac{f_1 \Delta P_1 + f_2 \Delta P_2}{f_1 + f_2}\right)/\lambda_{mw} \quad (3)$$

with $\lambda_{mw} = c/(f_1 - f_2)$ being the Wide-Lane (WL) wavelength, which is 0.86m for GPS&QZSS, 1.02m for BDS, 0.81m for Galileo and satellite dependent for GLONASS (roughly 0.8m). $\Delta N_{mw} = \Delta N_1 - \Delta N_2$ is the WL CS in cycle.

In case where the triple-frequency measurements are available, the TD EMW LC can be used to detect the CSs as:

$$\Delta N_{emw} = \left(\frac{f_2 \Delta L_2 - f_5 \Delta L_5}{f_2 - f_5} - \frac{f_2 \Delta P_2 + f_2 \Delta P_5}{f_2 + f_5}\right)/\lambda_{emw} \quad (4)$$

with $\lambda_{emw} = c/(f_2 - f_5)$ being the Extra WL (EWL) wavelength, which is 5.86m for GPS&QZSS, 4.88m for BDS, 9.77m for Galileo and satellite dependent for GLONASS. $\Delta N_{emw} = \Delta N_2 - \Delta N_5$ is the EWL CS in cycle. If equation (3) or (4) is larger than the threshold, e.g. 4 times of the corresponding measurement noise, a CS vector is detected.

Both equations (3) and (4) eliminate the effects of geometry clocks, hardware biases and atmospheric (especially the first order ionospheric) delays and they are very effective to detect

even one CS under a benign environment. However, the detection performance of equations (3) and (4) are dominated by the code noise (Li et al 2014), as presented in Tables 1 to 3 for satellite systems of GPS&QZSS, BDS and Galileo. Therefore, if the code measurement is noisy, such as under low elevation or heavy multipath scenarios, the measurement noise of equation (3) will be close or even more than one WL wavelength even if there is no CS. Equation (4), however, has much longer wavelength than equation (3) (see Tables 1 to 3) and the impact of code noise on equation (4) is almost the same as the code noise's impact on (3). Even though the phase noise increases by a factor of 30 (for GPS) in equation (4), it still has a smaller impact than the measurement noise in equation (3), which means more reliable detection results can be obtained using the TD EMW LC, especially for Galileo, which has an EWL wavelength of 9.77m (Table 3).

LC	Wavelength (m)	Noise (m)
L1, P1	0.1903	σ_L, σ_P
L2, P2	0.2442	σ_L, σ_P
L5, P5	0.2548	σ_L, σ_P
MW	0.8619	sqrt(33 σ_L^2+0.51σ_P^2)
EMW	5.8610	sqrt(1105 σ_L^2+0.50σ_P^2)

Table 1. GPS & QZSS wavelength and measurement noise

LC	Wavelength (m)	Noise (m)
B1, B1	0.1920	σ_L, σ_P
B2, B2	0.2483	σ_L, σ_P
B3, B3	0.2363	σ_L, σ_P
MW	1.0247	sqrt(47 σ_L^2+0.51σ_P^2)
EMW	4.8842	sqrt(814 σ_L^2+0.50σ_P^2)

Table 2. BDS wavelength and measurement noise. MW uses B1 and B3

LC	Wavelength (m)	Noise (m)
E1, E1	0.1903	σ_L, σ_P
E5a, E5a	0.2483	σ_L, σ_P
E5b, E5b	0.2548	σ_L, σ_P
MW	0.8140	sqrt(29 σ_L^2+0.51σ_P^2)
EMW	9.7684	sqrt(3017 σ_L^2+0.50σ_P^2)

Table 3. Galileo wavelength and measurement noise

Moreover, it is observed from equations (3) and (4) that if identical slip occurs on each frequency (even though the chances are small according to Blewitt (1990)), ΔN_{mw} or ΔN_{emw} will be equal to 0. Under such circumstances, the CSs cannot be detected using either equation (3) or (4). Therefore the TD GF LC can be used as a supplementary as:

$$\Delta L_{gf12} = \Delta L_1 - \Delta L_2 \quad (5a)$$
$$\Delta L_{gf15} = \Delta L_1 - \Delta L_5 \quad (5b)$$

If equation (5a) or (5b) is larger than four times of its corresponding measurement noise, then CS is considered to be detected.

Therefore, the whole LC-based approach can be summarized into the following steps: 1) if triple-frequency measurements are available, both equations (3) and (4) can be used to detect CSs on L1&L2 and L2 & L5, respectively, as long as the CS on each frequency is not the same; 2) in case of identical CSs on dual- or triple-frequency, equation (5a) or (5b) can be used. It is important to comment that CS detection is extremely difficult under noisy scenarios, such as low elevations.

QC approach

The CS detection can also be implemented based on the QC theory. The null and alternative hypotheses mathematical models can be described as follows:

$$l_i = A_i x + v_i \quad (6)$$
$$l_i = A_i x + B_i b_i + \varepsilon_i \quad (7)$$

with $l_i = [\Delta L_i \; \Delta P_i]$ being the measurement vector of the ith frequency, $A_i = \begin{bmatrix} 1 & -u_i \\ 1 & u_i \end{bmatrix}$ being the design matrix and $B_i = \lambda_i$. Vector x consists of TD non-dispersive unknowns and ionospheric delay. b is the CS vector to be estimated under the alternative hypothesis. Equation (5a) can be used to provide priori information on the TD ionospheric residual using previous epochs. If dual- or triple-frequency measurements are available, the corresponding design matrices of the alternative hypothesis (7) will be respectively:

$$A = \begin{bmatrix} 1 & u_1 & 0 & 0 \\ 1 & u_2 & 0 & 0 \\ 1 & -u_1 & \lambda_1 & 0 \\ 1 & -u_2 & 0 & \lambda_2 \\ 0 & 1 & 0 & 0 \end{bmatrix} \quad (8)$$

for dual-frequency, or

$$A = \begin{bmatrix} 1 & u_1 & 0 & 0 & 0 \\ 1 & u_2 & 0 & 0 & 0 \\ 1 & u_5 & 0 & 0 & 0 \\ 1 & -u_1 & \lambda_1 & 0 & 0 \\ 1 & -u_2 & 0 & \lambda_2 & 0 \\ 1 & -u_5 & 0 & 0 & \lambda_5 \\ 0 & 1 & 0 & 0 & 0 \end{bmatrix} \quad (9)$$

for triple-frequency.

Note that for the null hypothesis, only the first two columns in equations (8) and (9) are used as the design matrices. Comparing (9) to (8), it is evident that the model's strength increases with the triple-frequency measurements (more redundancy).

The CS detection is performed by checking the least-squares residuals of the null hypothesis as:

$$T = \hat{v}^T P \hat{v} \tag{10}$$

with P being the TD weight matrix for code, phase and ionosphere residual noise (see section 3). Equation (10) follows a χ^2 distribution and by specifying a significance level, e.g. alpha=0.001, the critical value can be derived. If T is larger than the threshold, potential model error need to be identified. If phase measurements have outliers, the CSs are detected and the alternative hypothesis model (7) can be used to estimate the float CS vector and its variance-covariance matrix.

2.2 The CS Repair step

Although in an LC-based approach, the integer rounding would be the most commonly used method to repair the CS to its nearest integer, it has been concluded that integer rounding achieves the lowest success-rate among integer rounding, integer bootstrapping and ILS (Teunissen 1998). The ILS is used instead of the integer rounding to repair the CS due to its optimal success rate.

Once the CSs are detected, the alternative model (7) can be directly applied to estimate the float CS vector $\hat{b}$ and its associated variance-covariance matrix $Q_{\hat{b}}$. In order to fix the float CS vector into integer, the Ps-Lambda (Teunissen 1995; Verhagen et al 2013) algorithm, is used.

3. EXPERIMENTAL RESULTS

In order to evaluate the performance of CS detection and repair algorithms, 1Hz data were collected from 9 MGEX stations (Montenbruck et al 2014) and 1 Australian CORS station, as plotted in Figure 1. Data sets from CUT0, TITG and TOW2 stations were logged by the authors' themselves from the corresponding mountpoints. The other data sets were concatenated from the high-rate data archived under ftp://igs.ign.fr/pub/igs/data/campaign/mgex/. Details of the data sets and GNSS systems and signals used are given in Table 4 and Table 5. It is worth mentioning that the data sets for TITG, CUT0 and TOW2 span only 6h.

During the testing, the phase noise variance was determined based on:

$$\sigma_L^2 = a^2 + b^2/\sin(el) \tag{11}$$

with a and b being set to 0.0015m and el representing the satellite elevation. The code noise was determined as $100\sigma_L$. Note that the measurement noise for BDS was slightly weighted by a factor of 1.2 (Teunissen and de Bakker 2013) and for GLONASS an empirical value of 1.5 was used. Only dual-frequency measurements for GLONASS were used. The elevation mask and TD ionosphere residual noise were set to 5 degree and 0.002m, respectively. The significance level for QC-based detection and pre-defined fail-rate for Ps-Lambda were set to 0.001 and 0.01 respectively.

Dataset	Date	Site	Receiver	Length	Network	Location	
						Lat	Lon
1	24.06.2016	ASCG	Trimble NetR9	24 h	MGEX	-7.916	-14.333
2	02.09.2016	CUT0	Trimble NetR9	6 h	MGEX	-32.004	115.895
3	24.06.2016	JFNG	Trimble NetR9	24 h	MGEX	30.516	114.491
4	24.06.2016	KOUG	Leica GR10	24 h	MGEX	5.098	-52.640
5	24.06.2016	METG	Trimble NetR9	24 h	MGEX	60.242	24.384
6	24.06.2016	RGDG	Trimble NetR9	24 h	MGEX	-53.786	-67.751
7	24.06.2016	SEYG	Trimble NetR9	24 h	MGEX	-4.679	55.531
8	02.09.2016	TITG	Sept PolaRx4TR	6 h	AUSCORS	-10.58	142.22
9	02.09.2016	TOW2	Sept PolaRx4TR	6 h	MGEX	-19.269	147.056
10	24.06.2016	YEL2	Sept PolaRx4TR	24 h	MGEX	62.481	-114.481

Table 4. Data sets descriptions

Site	Systems & signals used				
	GPS	GLONASS	BDS	GAL	QZS
	L1, L2, L5	L1, L2	B1, B3, B2	E1, E5a, E5b	L1, L2, L5
ASCG	1C, 2W, 5X	1P, 2P	2I, 6I, 7I	1X, 5X, 7X	-
CUT0	1C, 2W, 5X	1P, 2P	2I, 6I, 7I	1X, 5X, 7X	1C, 2X, 5X
JFNG	1C, 2W, 5X	1P, 2P	2I, 6I, 7I	1X, 5X, 7X	-
KOUG	1C, 2W, 5Q	1C, 2P	2I, 7I	1C, 5Q, 7Q	-
METG	1C, 2W, 5X	1P, 2P	2I, 6I, 7I	1X, 5X, 7X	-
RGDG	1C, 2W, 5X	1P, 2P	2I, 6I, 7I	1X, 5X, 7X	-
SEYG	1C, 2W, 5X	1P, 2P	2I, 6I, 7I	1X, 5X, 7X	-
TITG	1C, 2W, 5Q	1C, 2P	2I, 7I	1C, 5Q, 7Q	1C, 2L, 5Q
TOW2	1C, 2W, 5Q	1C, 2P	2I, 7I	1C, 5Q, 7Q	1C, 2L, 5Q
YEL2	1C, 2W, 5Q	1C, 2P	2I, 7I	1C, 5Q, 7Q	-

Table 5. Systems & signals used for testing

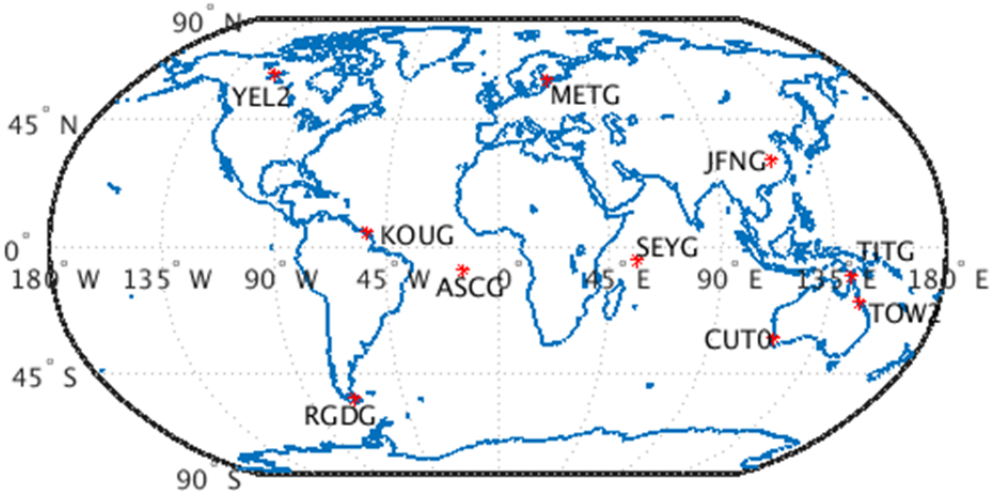

Figure 1. Geographical location of the stations used

3.1 The Benefits of Triple-Frequency

The data from the above 10 stations were processed for each GNSS and the results are shown in Figures 2 through 6. Note that for the purpose of the analysis, only GNSS satellites with

triple-frequency measurements were used, except for GLONASS. The 10-station TD EMW residuals are shown on the top left subfigures and the TD MW residuals are shown on the top right subfigures. The time-series for the TD EMW and the TD MW residuals exhibit different patterns, depending on the group of GNSS receivers and signals used. The residual patterns for GPS, Galileo and GLONASS, from the first epoch, follow the receiver types of Trimble, Leica, Trimble and Septentrio accordingly. The residual pattern for BDS is quite consistent, because of the same signals used, i.e., 1I, 6I and 7I, which come from the same Trimble receiver type (Tables 4 and 5) for all 6 stations. Finally, for QZSS the pattern follows Trimble and Septentrio.

Obviously, the TD EMW residuals are much smaller than the residuals of TD MW. As aforementioned, the reason is that, the EMW LC has a much longer wavelength than MW LC (Tables 1-3). The impacts of code noise on the MW LC and EMW LC are almost the same. The phase noise has a higher impact on the EMW LC than the MW LC, due to its larger coefficient (see Tables 1 to 3), but it still remains less prominent than the code's noise (dm-m).

The EMW residuals, due to their larger wavelength, exhibit better CS detection performance than the MW residuals according to Figures 2 to 5. In the lower subfigures of each figure (2-5), the probabilities of TD EMW residuals falling into the region of [-0.5 0.5] cycles are 100% for GPS, 99.98% for BDS, 100% for Galileo and 100% for QZSS. For the TD MW residuals, the probabilities are lower with 99.47% for Galileo, 97.59% for BDS, 94.15% for GPS, 93.03% for QZSS and 89.70% for GLONASS. Therefore, using TD EMW to detect CSs on L2 (and L5) provides more reliable results than using TD MW. Since the integer rounding success-rate of using TD EMW LC is sufficiently close to 100%, it may be used as additional information to enhance the algorithm.

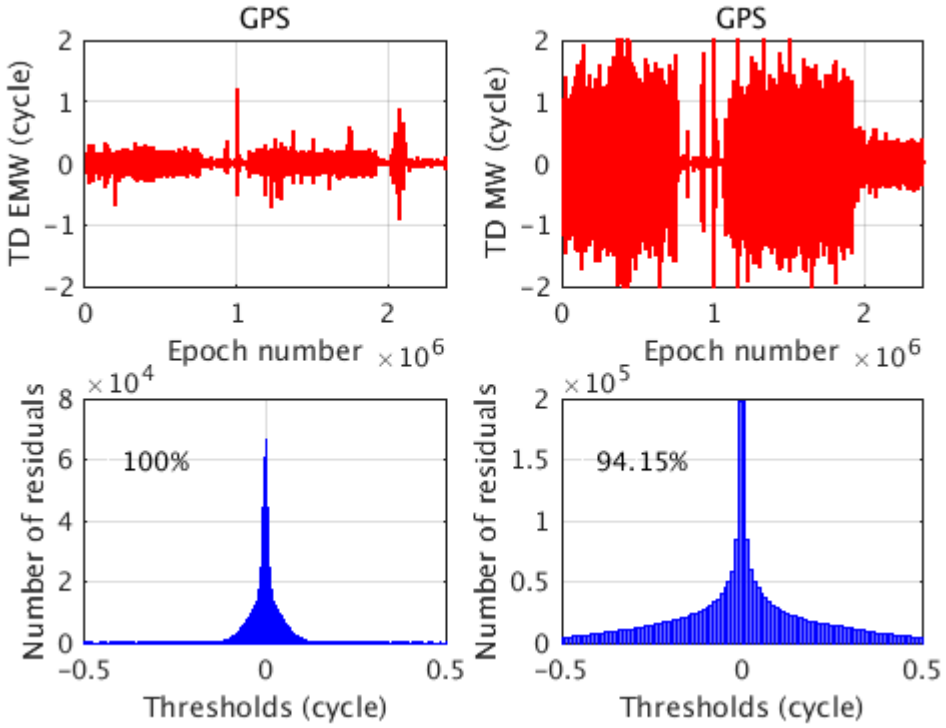

Figure 2. GPS TD EMW and TD MW noise analysis

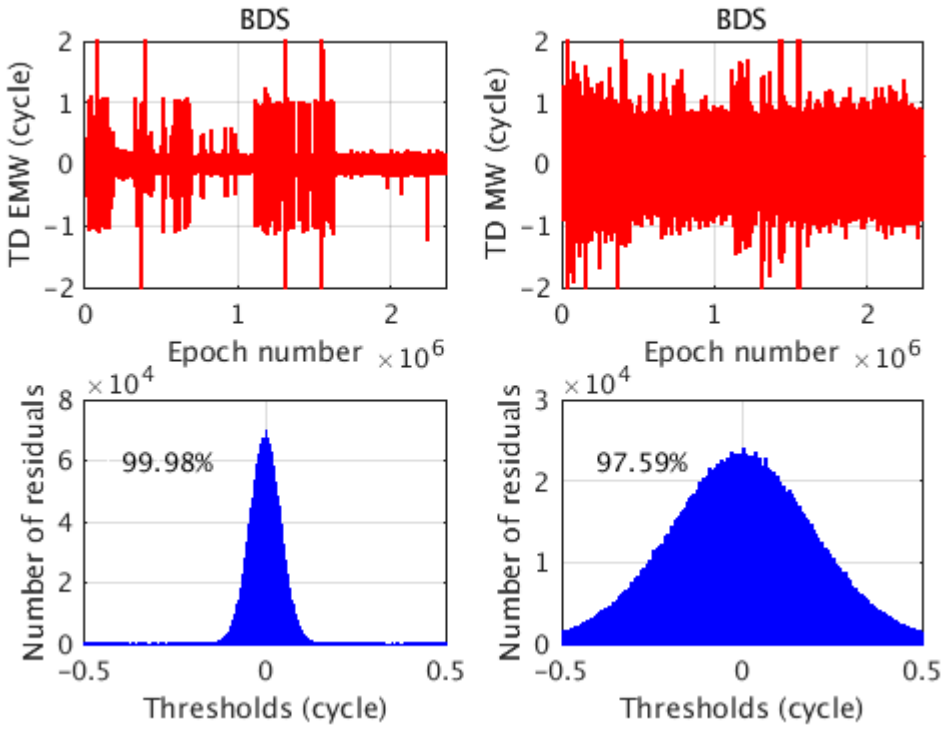

Figure 3. BDS TD EMW and TD MW noise analysis

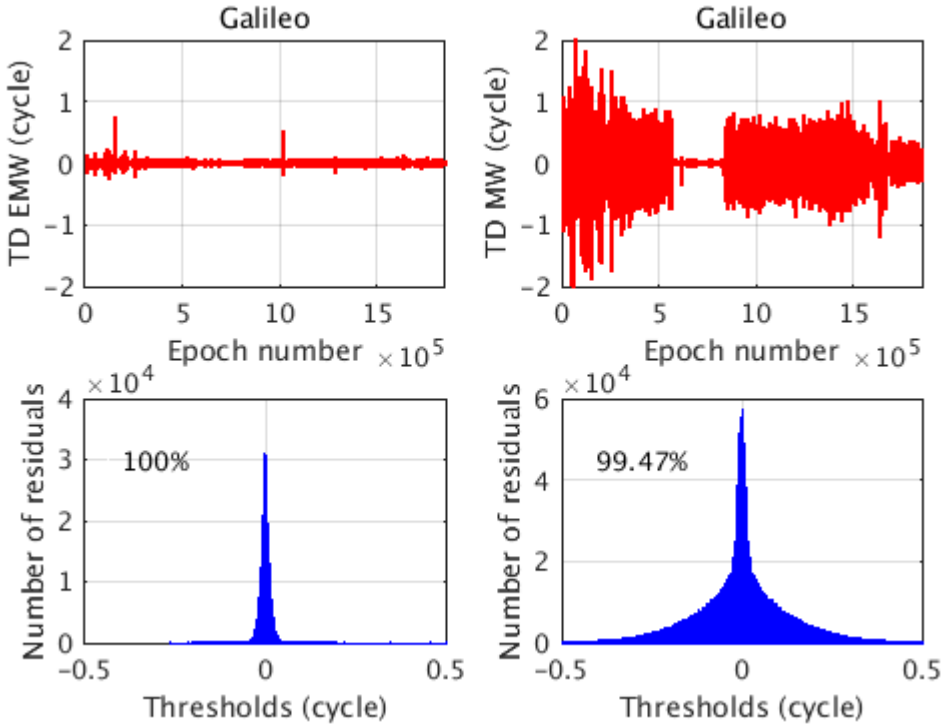

Figure 4. Galileo TD EMW and TD MW noise analysis

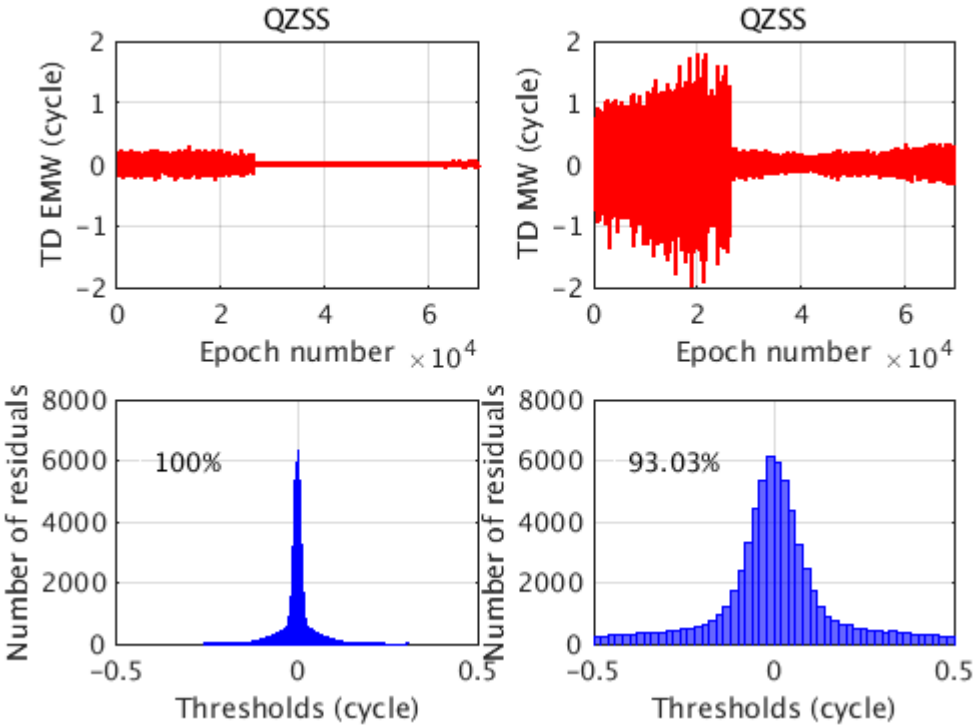

Figure 5. QZSS TD EMW and TD MW noise analysis

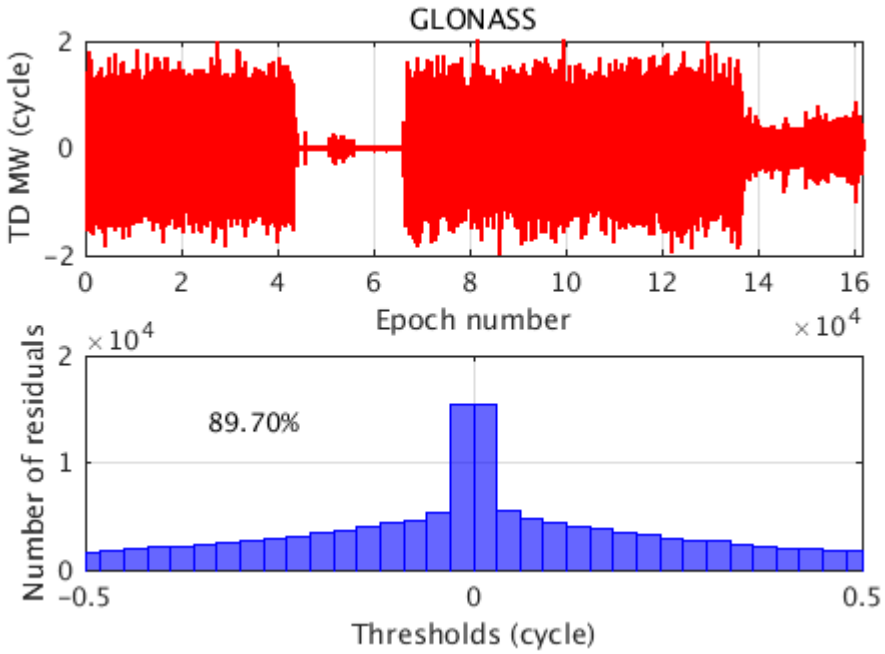

Figure 6. GLONASS TD MW noise analysis

3.2 Detection and Repair Results

To evaluate the CS detection and repair performance, one satellite from each GNSS system was chosen, namely G10 for GPS, R24 for GLONASS, C06 for BDS, E22 for Galileo and J01 for QZSS.

	Case 1 [1 1]		Case 2 [0 1]		Case 3 [9 7]	
	LC	QC	LC	QC	LC	QC
Detected	1382	1382	1382	1382	1304	1308
Repaired	1371	1371	1371	1371	1296	1300
Correct fixing	1371	1371	1371	1371	1296	1300
Wrong fixing	0	0	0	0	0	0
Truth	1382	1382	1382	1382	1382	1382

Table 6. CS detection and repair results for satellite G10 using dual-frequency

	Case 1 [1 1]		Case 2 [0 1]		Case 3 [9 7]	
	LC	QC	LC	QC	LC	QC
Detected	1049	1055	1072	1072	643	668
Repaired	860	860	860	860	555	571
Correct fixing	859	859	859	859	554	570
Wrong fixing	1	1	1	1	1	1
Truth	1142	1142	1142	1142	1142	1142

Table 7. CS detection and repair results for satellite R24 using dual-frequency

	Case 1 [1 1]		Case 2 [0 1]		Case 3 [9 7]	
	LC	QC	LC	QC	LC	QC
Detected	1662	1662	1662	1662	1396	1468
Repaired	1618	1618	1618	1618	1382	1453
Correct fixing	1618	1618	1618	1618	1382	1453
Wrong fixing	0	0	0	0	0	0
Truth	1662	1662	1662	1662	1662	1662

Table 8. CS detection and repair results for satellite C06 using dual-frequency

	Case 1 [1 1]		Case 2 [0 1]		Case 3 [9 7]	
	LC	QC	LC	QC	LC	QC
Detected	1589	1589	1589	1589	1481	1585
Repaired	1571	1571	1571	1571	1470	1569
Correct fixing	1571	1571	1571	1571	1470	1569
Wrong fixing	0	0	0	0	0	0
Truth	1589	1589	1589	1589	1589	1589

Table 9. CS detection and repair results for satellite E22 using dual-frequency

	Case 1 [1 1]		Case 2 [0 1]		Case 3 [9 7]	
	LC	QC	LC	QC	LC	QC
Detected	459	459	459	459	445	448
Repaired	456	456	456	456	444	447
Correct fixing	456	456	456	456	444	447
Wrong fixing	0	0	0	0	0	0
Truth	459	459	459	459	459	459

Table 10. CS detection and repair results for satellite J01 using dual-frequency

Then three verification case scenarios with vectors of [1 1 1], [0 1 0] and [9 7 0] for triple-frequency and [1 1], [0 1] and [9 7] for dual-frequency were artificially added as an integer number of cycles into the raw measurements of L1 (B1, E1 for BDS, Galileo), L2 (B2, E5a

for BDS, Galileo) and L5 (B3 and E5b for BDS, Galileo) accordingly. The CS vectors were introduced every 300 seconds starting from the first epoch of the measurements. The detection and repair results using dual-frequency only and triple-frequency (dual-frequency, in case there is no triple-frequency) are given in Tables 6-10, and 11-14, respectively. Only the epochs impacted from the introduced CS vectors (known ground truth) are analysed.

In the dual-frequency, the LC approach (based on the MW LC) and QC approach exhibit the same results for GPS, BDS, Galileo and QZSS in Cases 1 and 2, where all the artificial CSs can be detected and the majority of those can be repaired. For GLONASS, however, the detection step performs a little bit worse with 1049 out of 1142 epochs detected and 860 out of 1049 epochs repaired with one wrong fixing. For Case 3, the entire detection and repair performance are not as good as in the first two Cases. The reason is that for Cases 1 and 2, if the TD MW LC cannot detect the CS, the TD GF LC is used instead (Eq.(5a) or (5b)). Then the CSs will be detected if the phase measurements are not so noisy. However, for Case 3, the TD GF LC residual repeatability is almost at the phase measurement noise level, which yields that if TD MW LC cannot detect the CSs, TD GF LC probably cannot either.

While most of the artificial CS epochs were detected, there were many left which couldn't be repaired. Keeping in mind that only dual-frequency measurements were used and the elevation mask was set at 5 degree, it is reasonable to assume that the model strength or (and) data quality is not reliable enough for a successful integer CS fixing using the Ps-Lambda method. For example, the only one wrong fixing for GLONASS is caused by the noisy data for this epoch.

For triple-frequency CS detection and repair, the results for satellites G10 and J01 are extremely promising as shown in Table 11 and Table14. All the artificial CSs were detected, no matter the approach, LC-based or QC-based. The detected CSs were correctly fixed to the corresponding integer vectors. For satellite E22, identical detection and repair results were obtained using LC approach and QC approach. However, it is noticed that although all the artificial CSs were detected, 4 of them could not be repaired. The reason is that for these four epochs, the elevations were low as 8.62, 8.05, 8.01 and 8.07 degrees. The corresponding R-ratio values for those epochs were 1.96, 1.97, 3.02 and 2.38, respectively. The critical values derived from the Ps-Lambda look-up table were 3.10, 3.31, 3.32 and 3.07, respectively, which means that those four epochs had higher measurement noise. Hence the most likely integer CS vector could not be confidently separated from the second most likely integer CS vector. Thus, no fixing was performed to avoid wrong fixing.

The CS detection and repair results for satellite C06 are close to the performance of G10 and J01. For Cases 1 and 2, both LC and QC approaches detected all the artificial CSs and only 1 epoch was not repaired. The elevation for this epoch was 7.94 degree, with the calculated R-ratio of 3.31. However, the R-ratio critical value is 11.6, which implies the data quality is not good enough to have a reliable fixing. In Case 3, both LC and QC detection approaches produced not as good results as in Cases 1 and 2. It was found that all undetected epochs had only dual-frequency measurements available. Therefore, only the TD MW and TD GF LCs could be used to perform CS detection. Under low elevations, both the TD MW and TD GF residuals are smaller than 4 times of the corresponding measurement noise determined from equation (11) for the undetected epochs. Therefore, a realistic stochastic model is of importance for CS detection under low elevation scenarios. The QC detection also exhibits undetected epochs. Besides the size of the CSs, it is once again evident, that dual-frequency measurements only and low elevations (high measurement noise) weaken the model's ability

to perform a reliable detection.

Interestingly enough, there was no wrong fixing in any triple-frequency case.

	Case 1 [1 1 1]		Case 2 [0 1 0]		Case 3 [9 7 0]	
	LC	QC	LC	QC	LC	QC
Detected	1382	1382	1382	1382	1382	1382
Repaired	1382	1382	1382	1382	1382	1382
Correct fixing	1382	1382	1382	1382	1382	1382
Wrong fixing	0	0	0	0	0	0
Truth	1382	1382	1382	1382	1382	1382

Table 11. CS detection and repair results for satellite G10 using triple-frequency

	Case 1 [1 1 1]		Case 2 [0 1 0]		Case 3 [9 7 0]	
	LC	QC	LC	QC	LC	QC
Detected	1662	1662	1662	1662	1612	1627
Repaired	1661	1661	1661	1661	1612	1627
Correct fixing	1661	1661	1661	1661	1612	1627
Wrong fixing	0	0	0	0	0	0
Truth	1662	1662	1662	1662	1662	1662

Table 12. CS detection and repair results for satellite C06 using triple-frequency

	Case 1 [1 1 1]		Case 2 [0 1 0]		Case 3 [9 7 0]	
	LC	QC	LC	QC	LC	QC
Detected	1589	1589	1589	1589	1589	1589
Repaired	1585	1585	1585	1585	1585	1585
Correct fixing	1585	1585	1585	1585	1585	1585
Wrong fixing	0	0	0	0	0	0
Truth	1589	1589	1589	1589	1589	1589

Table 13. CS detection and repair results for satellite E22 using triple-frequency

	Case 1 [1 1 1]		Case 2 [0 1 0]		Case 3 [9 7 0]	
	LC	QC	LC	QC	LC	QC
Detected	459	459	459	459	459	459
Repaired	459	459	459	459	459	459
Correct fixing	459	459	459	459	459	459
Wrong fixing	0	0	0	0	0	0
Truth	459	459	459	459	459	459

Table14. CS detection and repair results for satellite J01 using triple-frequency

3.3 ILS Success-rate Analysis

The integer CS repair step is equivalent to the integer ambiguity resolution problem, which has been thoroughly researched and well-implemented in the Ps-Lambda software. To examine the reliability of the integer CS repair step, as shown in Figures 7 and 8, the approximate dual- and triple-frequency ILS success-rates were plotted against the satellite elevations. Obviously, the success-rate relies heavily on the satellite elevation and the number

of frequencies used. For triple-frequency, when the elevation is higher than 30 degree, the success-rates of satellites G10, E22 and J01 are all sufficiently close to 100%. For satellite C06, about the first 1200 epochs indicate 100% success-rate, but for the remaining last epochs lower success-rates are attained mainly because only dual-frequency measurements were available.

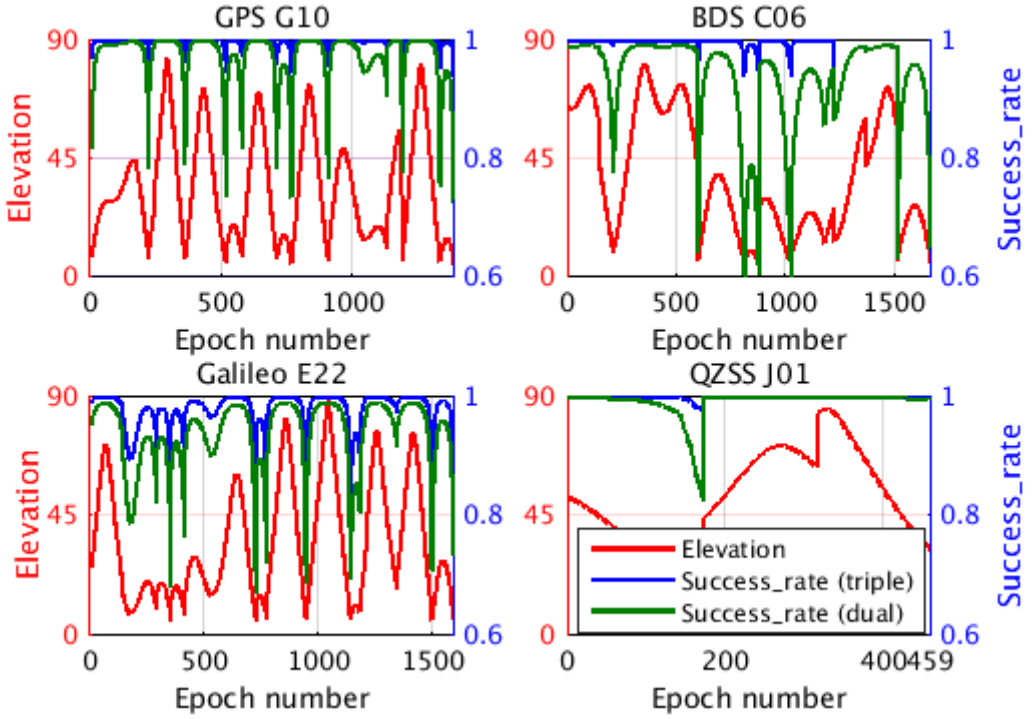

Figure 7. ILS success-rates versus satellite elevations for CDMA based satellite systems

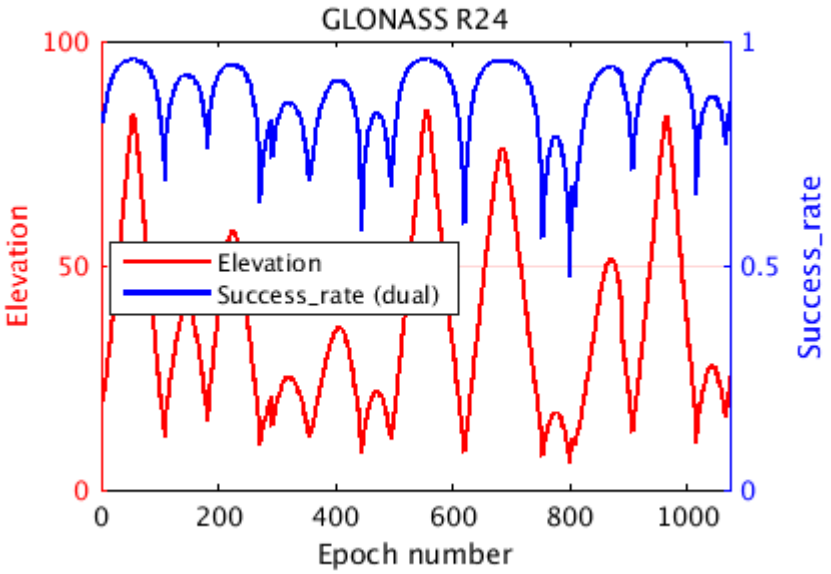

Figure 8. ILS success-rate versus satellite elevation for GLONASS (FDMA)

In the dual-frequency case, as illustrated by the brown lines, the success-rates are lower than

the triple-frequency counterpart, especially when satellite elevation is low. It is obvious, that not only the data quality, but also, the model's strength is indispensable factors for a reliable repair.

4. CONCLUSIONS

CS detection and repair are essential quality control steps in the use of high-precision carrier phase measurements. In this contribution, the commonly used LC-based approach and QC-based approach for detection are comparatively studied. Contrary to other studies, these approaches were applied in the real-time network domain. The results clearly indicate the effectiveness and benefits of using the TD EMW triple-frequency LC over TD MW dual-frequency LC and more enhanced algorithms could be developed based on this conclusion.

In terms of actual CS detection and repair performance, both the LC- and QC-based approaches show satisfactory (less satisfactory) results using triple-frequency (dual-frequency) measurements.

The Ps-Lambda method is used for CS repair rather than the integer rounding approach since it is more optimal and its success-rate is higher. The results show the reliability of the repair approach with zero wrong fixings in the triple-frequency case and only 1 wrong fixing in the dual-frequency case. It is clear that the triple-frequency measurements ensure much stronger model to perform both a reliable detection and repair (fixing) of the CSs.

However, under lower elevations with higher measurement noise and rapid ionosphere fluctuations, CS detection and repair remains a challenging domain. Future work will focus on those issues.

ACKNOWLEDGEMENTS

This work has been supported by the Cooperative Research Centre for Spatial Information, whose activities are funded by the Business Cooperative Research Centres Programme. The International GNSS Real-Time Service (IGS-RT) and Multi-GNSS Experiment (MGEX) station providers are also acknowledged.

REFERENCES

Baarda W (1968) A testing procedure for use in geodetic networks, *Publications on Geodesy*, New Series 2, vol5, Netherlands Geodetic Commission, Delft.

Banville S, Langley RB (2013) Mitigating the impact of ionospheric cycle slips on GNSS observations, *Journal of Geodesy*, 87:179-193.

Bisnath SB, Langley RB (2000) Automated cycle-slip correction of dual-frequency kinematic GPS data, *In: Proceedings of 47th Conference of CASI*, Ottawa, Canada.

Blewitt G (1990) An automatic editing algorithm for GPS data, *Geophysical Research Letters*, 17(3):199-202.

Euler HJ, Schaffrin B (1990) On a measure for the discernibility between different ambiguity solutions in the static-kinematic GPS-mode, *IAG Symposia, no. 107. In: Kinematic systems in geodesy, surveying, and remote sensing*, Springer, New York, 285-295.

Gao Y, Li Z (1999) Cycle slip detection and ambiguity resolution algorithms for dual-frequency GPS

data processing, *Marine Geodesy*, 22(4): 169-181.

Kim D, Langley RB (2001) Instantaneous real-time cycle slip correction of dual-frequency GPS data, *In: Proceedings of the international symposium on kinematic systems in geodesy, geomatics and navigation*, Banff, Alberta, Canada, 255-264.

deLacy MC, Reguzzoni M, Sanso F (2012) Real-time cycle slip detection in triple-frequency GNSS, *GPS Solutions*, 16(3): 353-362.

Hatch R (1983) The synergism of GPS code and carrier phase measurements. *International Geodetic symposium on satellite Doppler positioning*, 2: 1213-1231.

Li T, Wang J, Laurichesse D (2014) Modelling and quality control for reliable precise point positioning integer ambiguity resolution with GNSS modernization, *GPS Solutions*, 18(3): 429-442.

Liu X, Tiberius CCJM, de Jong K (2004) Modelling of differential single difference receiver clock bias for precise positioning, *GPS Solutions*, 4:209-221.

Liu ZZ (2011) A new automated cycle slip detection and repair method for a single dual-frequency GPS receiver, *Journal of Geodesy*, 85: 171-183.

Melbourne W (1985) The case for ranging in GPS based geodetic systems, *Proceedings of first international symposium on precise positioning with global positioning system*, Rockville, 15-19, April, 373-386.

Montenbruck O, Steigenberger P, Khachikyan R, Weber G, Langley RB, Mervart L, Hugentobler U (2014) IGS-MGEX: Preparing the Ground for Multi-Constellation GNSS Science, *Inside GNSS* 9(1): 42-49.

Odijk D, Verhagen, S (2007) Recursive Detection, Identiciation and Adaption of model errors for reliable high-precision GNSS positioning and attitude determination, in: *3rd international conference on recent advances in space technologies (RAST '07)*, Istanbul, 624-629.

Teunissen PJG (1990) An integrity and quality control procedure for use in multi sensor integration, *Proceedings of ION GPS-90*, pp. 513-522, Colorado Springs, CO, September 19-21, 1990.

Teunissen PJG (1995) The least-squares ambiguity decorrelation adjustment: a method for fast GPS integer estimation, *Journal of Geodesy*, 72(10): 606-612.

Teunissen PJG, de Bakker PF (2013) Single-receiver single-channel multi-frequency GNSS integrity: outliers, slips, and ionospheric disturbances, *Journal of Geodesy*, 87:161-177.

Teunissen PJG, de Bakker PF (2015) Multivariate integer cycle-slip resolution: a single-channel analysis, *VIII Hotine-Marussi Symposium on Mathematical Geodesy, IAG Symposia*, 142:33-39.

Verhagen S, Li B, Teunissen PJG (2013) Ps-LAMBDA: ambiguity success rate evaluation software for interferometric applications, *Computers & Geosciences*, 54: 361-376.

Wübbena G (1985) Software developments for geodetic positioning with GPS using TI-4100 code and carrier measurements, *Proceedings of first international symposium on precise positioning with global positioning system*, Rockville, 15-19, April, 403-412.

Zhang XH, Li P (2015) Benefits of the third frequency signal on cycle slip correction, *GPS Solutions*, 20(3): 451-460.

Zhao QL, Sun BZ, Dai ZQ, Hu ZG, Shi C, Liu JN (2015) Real-time detection and repair of cycle slips in triple-frequency GNSS measurements, *GPS Solutions*, 19:381-391.